Spectrochimica Acta Part A: Molecular and Biomolecular Spectroscopy 278 (2022) 121300

Contents lists available at ScienceDirect

Spectrochimica Acta Part A: Molecular and Biomolecular Spectroscopy

journal homepage: www.elsevier.com/locate/saa

Spectroscopic investigation of the electronic and excited state properties of para-substituted tetraphenyl porphyrins and their electrochemically generated ions

Lauren Hanna [a], Edgar Movsesian [b], Miguel Orozco [b], Anthony R. Bernot Jr. [b], Mona Asadinamin [c], Learnmore Shenje [c], Susanne Ullrich [c], Yiping Zhao [c], Nicholas Marshall [d], Jason A. Weeks [e], Michael B. Thomas [a], Joseph A. Teprovich Jr. [b,*], Patrick A. Ward [a,*]

[a] Advanced Manufacturing and Energy Science, Savannah River National Laboratory, Aiken, SC 29803, USA
[b] Department of Chemistry and Biochemistry, California State University Northridge, 18111 Nordhoff St., Northridge, CA 91330, USA
[c] Department of Physics and Astronomy, University of Georgia Athens, GA, USA
[d] Department of Chemistry and Physics, University of South Carolina-Aiken Aiken, SC, USA
[e] College of Natural Sciences, University of Texas Austin, Austin, TX, USA

HIGHLIGHTS

- Photoelectrochemical spectra of substituted free base porphyrins were collected.
- Influence of porphyrin substitutions on excited state kinetics were investigated.
- Fluorescence profiles of ionic porphyrin species are reported.
- Time-dependent density functional theory was used to compare electronic structure.

GRAPHICAL ABSTRACT

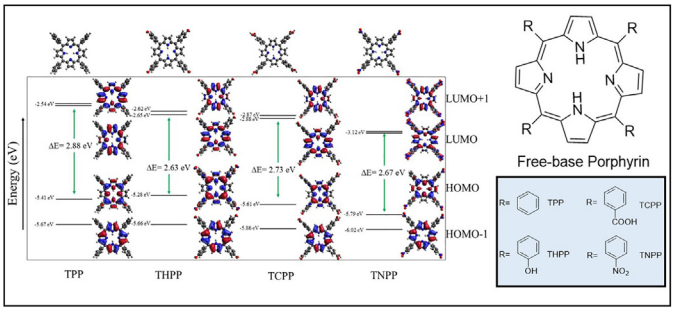

ARTICLE INFO

Article history:
Received 4 January 2022
Received in revised form 20 April 2022
Accepted 22 April 2022
Available online 29 April 2022

ABSTRACT

Porphyrins play pivotal roles in many crucial biological processes including photosynthesis. However, there is still a knowledge gap in understanding electronic and excited state implications associated with functionalization of the porphyrin ring system. These effects can have electrochemical and spectroscopic signatures that reveal the complex nature of these somewhat minor substitutions, beyond simple inductive or electronic effect correlations. To obtain a deeper insight into the influences of porphyrin functionalization, four free-base, *meso*-substituted porphyrins: tetraphenyl porphyrin (TPP), tetra(4-hydroxyphenyl) porphyrin (THPP), tetra(4-carboxyphenyl) porphyrin (TCPP), and tetra(4-nitrophenyl) porphyrin (TNPP), were synthesized, characterized, and investigated. The influence of various substituents, (-hydroxy,-carboxy, and -nitro) in the para position of the *meso*-substituted phenyl moieties were evaluated by spectroelectrochemical techniques (absorption and fluorescence), femtosecond transient absorption spectroscopy, cyclic and differential pulse voltammetry, ultraviolet photoelectron spectroscopy (UPS), and time-dependent density functional theory (TD-DFT). Spectral features were evaluated for the neutral porphyrins and differences observed among the various porphyrins were further explained using rendered frontier molecular orbitals pertaining to the relevant transitions. Electrochemically generated anionic and cationic porphyrin species indicate similar absorbance spectroscopic signatures attributed to a red-shift in the Soret band. Emissive behavior reveals the emergence of

* Corresponding authors at: Savannah River National Laboratory, Aiken, SC 29803, USA (P.A. Ward). California State University Northridge, Northridge, CA 91330, USA (J.A. Teprovich).
E-mail addresses: joseph.teprovich@csun.edu (J.A. Teprovich Jr.), patrick.ward@srnl.doe.gov (P.A. Ward).

https://doi.org/10.1016/j.saa.2022.121300
1386-1425/

one new fluorescence decay pathway for the ionic porphyrin, distinct from the neutral macrocycle. Femtosecond transient absorption spectroscopy analysis provided further analysis of the implications on the excited-state as a function of the para substituent of the free-base *meso*-substituted tetraphenyl porphyrins. Herein, we provide an in-depth and comprehensive analysis of the electronic and excited state effects associated with systematically varying the induced dipole at the methine bridge of the free-base porphyrin macrocycle and the spectroscopic signatures related to the neutral, anionic, and cationic species of these porphyrins.

1. Introduction

One of the greatest scientific challenges society faces is meeting the ever-growing energy demand while minimizing the global carbon footprint of energy production. To address this, the utilization of solar energy has been vigorously pursued as it represents the largest renewable energy resource available to our planet. A variety of chromophores, which model biological complexes, have been investigated in the pursuit of a means of efficient solar radiation conversion into a use form for societal utilization.[1–2] However, there are several requirements of these light collecting antennas which enable them to effectively transform solar energy. While visible light absorption is an important characteristic, it is equally imperative that the photophysical properties of the chromophore are conducive to efficient charge separation and transfer so that this class of biologically-relevant complexes can lead to the production of a viable and efficient source of energy.

Nature offers examples of highly efficient chromophores that can serve as inspiration for solar technology. For example, chlorins are naturally occurring tetrapyrrolic macrocycles and the main component of Chlorophyll *A* and Chlorophyll *B* which drive photosynthesis through a series electron transfer processes.[3] Similarly, porphyrins are tetrapyrrolic complexes known to be structurally robust. These macrocycles exhibit high molar absorptivity within the visible and UV wavelengths allowing efficient utilization of a large portion of the solar spectrum.[1] Furthermore, porphyrins permit facile functionalization, which enables one to fine-tune their photophysical properties for tailored natural light harvesting applications. This customizable structure–function relationship is inherently attractive; however, additional analysis is needed to understand the aspects that govern electron and energy transfer mechanisms required for the development of porphyrins as suitable chromophores in devices.

Previous work has been conducted on a range of free-base porphyrins substituted with various substituent groups.[4–5] However, no prior study has provided a comprehensive investigation of excited-state and electronic effects due to *meso*-substitution with substituents of different chemical identities. The fundamental investigation reported herein aims to generate foundational insights that will create a detailed picture of the structure–function relationship for a series of *meso*-substituted phenyl free-base porphyrins with *para*-phenyl substituents. The electronic structure and photophysical properties of the "parent" 5,10,15,20-tetra (phenyl) porphyrin (TPP), is compared to 5,10,15,20-tetra(4-carbox yphenyl) porphyrin (TCPP), 5,10,15,20-tetra(4-nitrophenyl) porphyrin (TNPP), and 5,10,15,20-tetra(4-hydroxyphenyl) porphyrin (THPP); each containing substituents in the *para*-position of the *meso*-phenyl groups. For reference, the molecular structures of these porphyrins are shown in Fig. 1.

The spectroscopic studies conducted using UV/Vis spectroscopy and femtosecond transient absorption spectroscopy, revealed electronic and excited state effects related to the nature of the *meso*-substitution. With the aid of time-dependent density functional theory (TD-DFT), theoretical spectra and rendered frontier molecular orbitals offer a deeper explanation for the spectral results, indicating how the peripheral decoration of the macrocycle results in varying degrees of stabilization based on the relevant electron density of the participating orbitals. Anionic and cationic species of the porphyrins were examined using spectroelectrochemical UV/Vis and emission spectroscopy to provide insight into the porphyrin ions by probing spectral signature information relevant to charge transfer processes. The investigation of charged porphyrins is necessary to understand the mechanistic process for how these model compounds for biologically relevant chromophores could serve as organic sensitizers within a photoelectrochemical device.

2. Experimental

2.1. Materials

Benzaldehyde (>99.5%), 4-hydroxybenzaldehyde (98%), p-nitrobenzaldehyde (98%), 4-formylbenzoic acid (97%), pyrrole (98%), acetone (>99.5%) and propionic acid (>99.5%) were all obtained from Sigma-Aldrich. Pyrrole was vacuum distilled to afford a colorless reagent before use. All other aldehydes and solvents were used without further purification. Meso-substituted porphyrins were synthesized via the Alder method and purified as needed by column chromatography or washing with cold acetone.[6] Additional synthetic details can be found in the supporting information. For electrochemical measurements, anhydrous and inhibitor-free tetrahydrofuran (THF) (>99.5%, Sigma-Aldrich) and tetrabutylammonium hexafluorophosphate ($TBAPF_6$) (electrochemical grade, Fluxa Analytical) were used. All sample preparations for electrochemical measurements were carried out in argon-filled glovebox to prevent moisture and oxygen exposure from influencing the measurements.

2.2. Ultraviolet photoelectron spectroscopy (UPS)

Ultraviolet photoelectron spectroscopy (UPS) was obtained utilizing a monochromated helium discharge lamp [HEI] (E = 21.22 e V), hybrid optics (employing a magnetic and electrostatic lens simultaneously) and a multi-channel plate coupled to a hemispherical photoelectron kinetic analyzer. Pressure of the analysis chamber was maintained at 2×10^{-9} Torr throughout the analysis. In order to assure that the samples did not charge during analysis a charge neutralizer was employed, alongside a 1.0 eV polarization. This setup thereby makes the effective energy of the beam 22.22 eV. This value was used in the experimental calculation of HOMO energy levels for the various porphyrin analogs. The spectra were calibrated by using Ag control to assure that energy levels were not influenced by the charge neutralization settings or any adventitious carbon in the chamber. The photoelectron take-off angle was normalized to the surface of the sample and 45° with respect to the source. All spectra were recorded using one sweep and an aperture slot of 300×700 μm^2. Spectra were collected employing a pass energy of 80 eV and 1 eV per step. Regions were collected using a pass energy of 20 eV and 0.1 eV per step with a

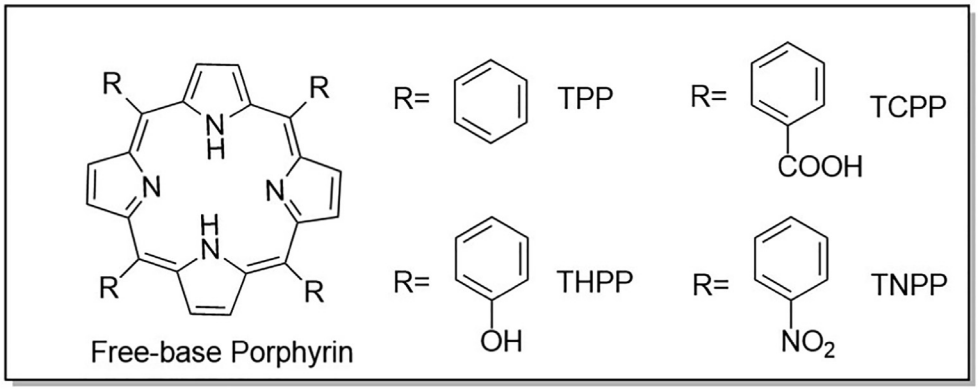

Fig. 1. Molecular structure of free-base Porphyrin and the *meso*-substitutuents evaluated in this work.

total acquisition time ranging from 10 to 12 min. CasaXPS software was employed to analyze the resulting spectra.

2.3. Nuclear magnetic resonance (NMR)

^{1}H and ^{13}C NMR spectra of porphyrins were acquired on a Bruker Avance III-D 400 MHz instrument in deuterated solvents as indicated, with residual solvent used as internal reference. Typical ^{1}H spectra were acquired as the sum of 16 transients, while ^{13}C spectra were the sum of 1024 transients.

2.4. Cyclic voltammetry (CV) and differential pulse voltammetry (DPV)

Cyclic voltammetry measurements were performed on air-free porphyrin solutions prepared in an argon filled glovebox. The samples were prepared by dissolving the desired porphyrin in deaerated and anhydrous THF with a tetrabutylammonium hexafluorophosphate ($TBAPF_6$) supporting electrolyte to generate a THF solution with a porphyrin to electrolyte concentration in 1:100 M ratio.

The measurements were conducted in a 50 mL, 3-neck round bottom flask with a Pt counter electrode, glassy carbon working electrode, and silver wire as a pseudo-reference electrode. The electrodes were immersed in the solution but sealed airtight to prevent re-oxidation of the reduced species during the measurement. Measurements were carried out on a BioLogic potentiostat controlled by EC-Lab software (BioLogic). The measured oxidation and reduction potentials were corrected with an internal ferrocene reference measured after the initial CVs. DPVs were recorded in a similar fashion.

2.5. Spectroelectrochemistry and electrochemical fluorescence spectroscopy

All samples were stored and prepared in an argon filled glovebox. UV/Vis was performed on a Cary 60 (Agilent Technologies) and fluorescence measurements were performed on a FS5 spectrophotometer (Edinburgh Instruments). The spectroelectrochemical UV/Vis and fluorescence measurements for the anionic and dianionic porphyrins were performed in home-made 4-sided quartz cell with a screw cap and airtight feedthroughs for the electrodes. The spectroelectrochemical UV/Vis and fluorescence measurements used a VMP3 potentiostat (BioLogic) with a Pt mesh working electrode, Pt wire counter electrode, and a silver wire as a pseudo reference electrode. The supporting electrolyte was $TBAPF_6$ in THF (0.1 M). Measurements for the generation of the dicationic species were conducted on a Lambda 45 spectrometer using a Pine Wave potentiostat with a Pt working electrode and counter electrode and a silver wire pseudo reference electrode.

Steady-state excitation and emission spectra were also collected on an Edinburgh FS5 spectrophotometer using a similar experimental setup as described above. A potential was applied accordingly to produce the desired cationic or anionic species. The emission spectrum was collected using the most intense wavelength from the UV/Vis data for the neutral, anionic, or cationic species for excitation. The excitation spectra were collected by monitoring the wavelengths of light that gave rise to the emission maximum for the neutral, anionic, and cationic species.

2.6. Femtosecond transient absorption spectroscopy

All transient absorption spectroscopy (TAS) experiments were performed with a HELIOS Fire (Ultrafast Systems) transient absorption spectrometer. The pump and probe sources were provided by a Ti:sapphire amplifier (Astrella, Coherent) with wavelength centered at 800 nm, pulse duration of 80 fs, and repetition rate of 5 kHz. The pump pulses were generated by splitting part of the 800 nm source light, one for the pump and another for the probe, in an optical parametric amplifier (OPA; Apollo, Ultrafast Systems), where it was converted to $\sim$ 418 nm light by using the fourth harmonic idler ($\sim$7 μJ). The experimental setup required the use of two choppers, one for the pump and one for the probe, to prevent continuous pumping and subsequent probing of a sample with long-lived luminescence. The probe was generated by using a CaF_2 crystal that generated the white light continuum (400–780 nm) generated from a portion of the fundamental 800 nm. The relative optimal overlap of the pump and probe pulses was adjusted for each sample to obtain the maximum signal. The transient absorption data were recorded on a HELIOS Fire spectrometer (Ultrafast Systems) coupled with a 8 ns delay line that translated the probe pulse. The change in absorbance measured for each sample was calculated as follows:

$$\Delta A(mOD) = -\log\left(I_{on}/I_{off}\right) * 1000 \quad (1)$$

The porphyrin samples were prepared by dissolving the solid in THF to reach a concentration of $\sim 10^{-5}$M porphyrin. The solution was analyzed using UV/Vis spectroscopy to ensure sufficient absorbance of the Soret band. All porphyrin solutions were measured in a 2 mm quartz cuvette with a magnetic stirrer to agitate the solution continuously. The UV/Vis spectra were collected following each experiment to confirm the quality of the sample.

The data were processed using Surface Xplorer.[7–9] Global analysis was performed using an instrument response function

(IRF) of 200 fs and decay associated spectra (DAS) were constructed. All data were chirp corrected and time zero corrected within Surface Xplorer.

2.7. Computational details

Geometry optimizations and time-dependent density functional theory (TD-DFT) calculations were performed using the Gaussian 16 platform.[10] Initially, substituted porphyrins were modeled in Avogadro[11–12] to generate the starting coordinates for the geometry optimization. The molecular structures were optimized using the B3LYP hybrid functional[13–16] and triple zeta 6-311G Pople basis set[17] with polarization functions on all atoms. To account for solvation, self-consistent reaction field methods were employed using the integral equation formalism polarizable continuum model (IEFPCM) with input parameters for tetrahydrofuran from the Gaussian 16 program. Previous work has demonstrated successful excited state predictions utilizing this functional and basis set for tetrapyrrole molecules.[18] Excited state calculations were performed on the optimized species using the same functional and basis set. The number of calculated transitions was set to 20. Singlet and triplet excitations were calculated separately for each TD-DFT calculation. Results were visualized and molecular orbitals were rendered using GaussView 6.[19] Transition dipole spectra were generated and broadened to match the experimental broadening. The excited state transitions of the highest oscillator strength were analyzed, and the highest contributing orbitals were rendered.

3. Results and discussion

3.1. UV/Vis spectroscopy

The absorption spectra of the *meso*-substituted porphyrins are shown in Fig. 2. The most intense absorption band < 450 nm corresponds to the Soret (or B) band whereas the low intensity absorption bands > 450 nm, are known as Q-bands.[20–22] These electronic transitions arise from pseudo dipole allowed or forbidden π-π^* transitions residing on the porphyrin macrocycle. The weakly absorbing Q-bands are HOMO-LUMO excitations that arise along the four-fold symmetry proton-axis found in free-base porphyrins; these are known as the Q_y and Q_x bands. Vibronic coupling generates a further split of these Q-band, giving rise to $Q_{x(0,0)}$, $Q_{x(0,1)}$, $Q_{y(0,0)}$, and $Q_{y(0,1)}$ named based on the initial and final vibronic states.[23].

The experimentally observed energies of the Soret and Q-bands for the parent porphyrin, TPP, are consistent to what has been reported for similar tetrapyrrole macrocycles.[24–26] In comparison, there is a noticeable red-shift in all Q-bands for THPP, as reported in Table 1. However, TNPP and TCPP only reveal a slight red-shift in the Soret band and little influence on the other transitions, with respect to TPP.

To deconvolute the experimentally observed spectral shifts among the porphyrins, the theoretical transition dipole spectra were computed and the relevant molecular orbitals were rendered to understand the nature of the underlying transitions. The theoretical spectra for each geometry optimized porphyrin were generated using time-dependent density functional theory (TD-DFT). As shown in Figure SI 1, the lack of substantial shifts in the calculated Soret band among the porphyrins is in reasonable agreement with the experimentally observed trends. Only the two symmetry separated Q-bands, Q_y and Q_x[27] are observed for TPP, TCPP, and THPP, while TNPP appears to have some supplementary transitions that may correspond to the additional Q-bands.

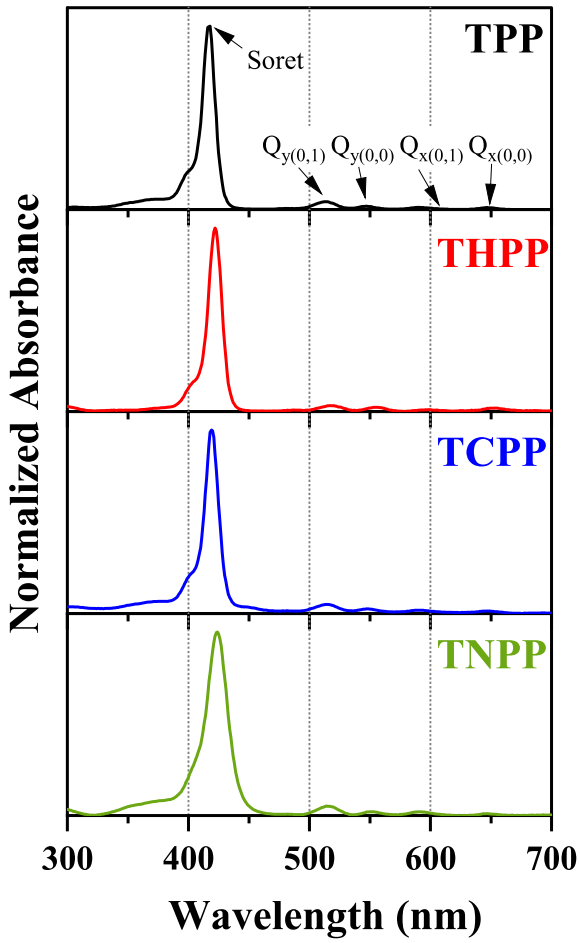

Fig. 2. UV/Vis spectra of TPP (black), THPP (red), TCPP (blue), and TNPP (green) measured in THF.

In Fig. 3, the orbitals pertaining to the transitions of highest oscillator strength are shown. As expected, these relevant orbitals were assigned to be the HOMO-1, HOMO, LUMO, and LUMO + 1 for all of the porphyrins. The TD-DFT calculations performed are also in excellent agreement with the experimental electronic structure measurements performed by UPS and UV/Vis (Figure SI 2–5). The rendered molecular orbitals representing the HOMO, LUMO, and LUMO + 1, reveal localized electron density on most or all methine bridges linking the pyrrolic units, as mapped by the blue and red lobes which correspond to the spin down and spin up orbitals, respectively. This suggests that transitions to and from these frontier orbitals may be more directly impacted by an inductive effect of the functional group near that position. In contrast, the HOMO-1 has no obvious electron density at any of the methine positions on the macrocycle. Provided this, the experimental shifts in the UV/Vis peaks can be elucidated. Figure SI 6 assigns the underlying transitions for Soret and Q-bands based on the TD-DFT calculations. The calculated peak < 450 nm has character from both the HOMO → LUMO + 1 and the HOMO-1 → LUMO + 1 transitions. The two calculated Q-bands are excitations from the HOMO-1 → LUMO (Q_y) and HOMO → LUMO (Q_x).

The relative energies of the rendered calculated frontier molecular orbitals offer a more comprehensive look as to how the various substituents affect the overall electronic structure. As illustrated in Fig. 3, there are distinct observations in the energy levels of the substituted porphyrins. The HOMO-1 molecular orbital, despite having no calculated electron density in the meso position, exhibits a reduction in energy with the substitution of

Table 1
UV/Vis Absorption bands of Neutral Porphyrins measured in THF.

Porphyrin	Soret (nm)	$Q_{y(0,1)}$ (nm)[a]	$Q_{y(0,0)}$ (nm)[a]	$Q_{x(0,1)}$ (nm)[a]	$Q_{x(0,0)}$ (nm)[a]
TPP	418	514	547	591	647
TCPP	419	514	549	590	647
TNPP	422	514	550	591	647
THPP	422	520	557	598	651

[a] assignment of Q-bands given by ref. [28].

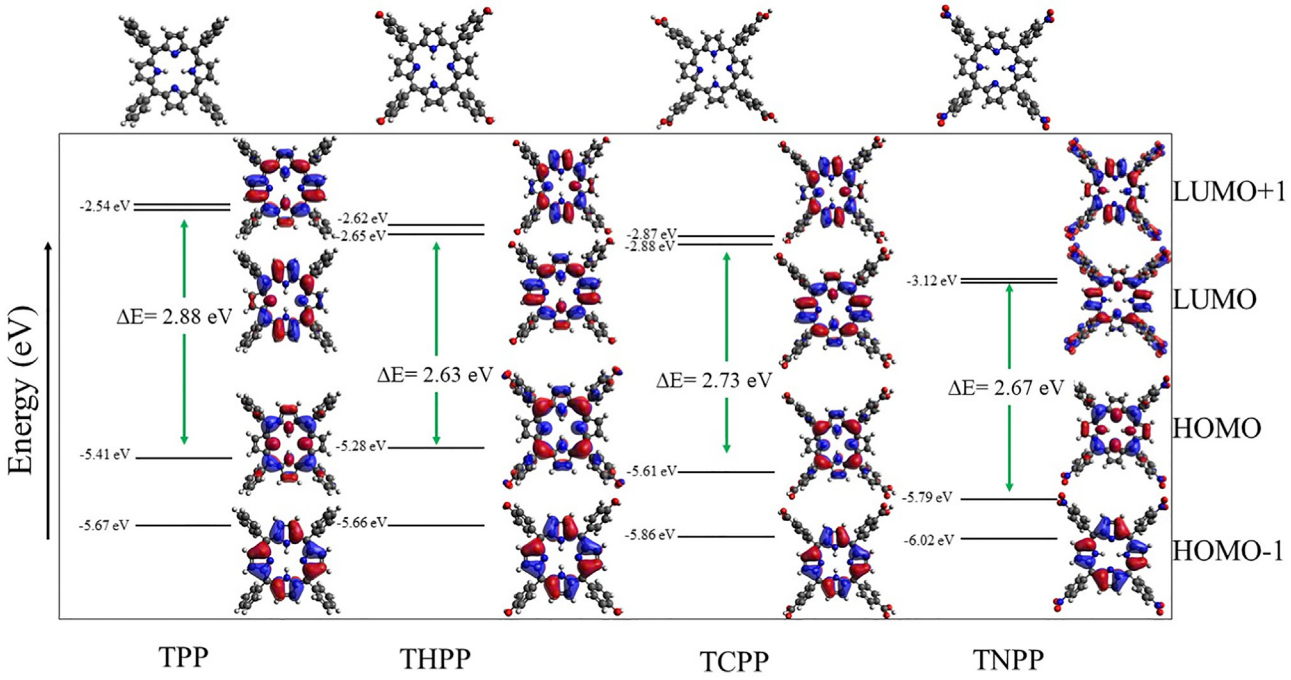

Fig. 3. TD-DFT calculated molecular orbitals of the relevant frontier orbitals for the *meso*-substituted porphyrins.

carboxy or nitro groups (–NO_2, –COOH) on the phenyl ring but not by the introduction of hydroxy (–OH). Compared to the parent, TPP, the energy of the HOMO is slightly increased in THPP in contrast to the reduction in energy observed for TNPP and TCPP. The unoccupied frontier orbitals reveal different effects than the occupied orbitals. Regardless of identity, all of the investigated *meso*-substituted porphyrins have nearly degenerate, LUMO and LUMO + 1. Notably, the porphyrin with hydroxyphenyl groups result in a larger reduction in the band gap compared to TCPP and TNPP, relative to TPP. These theoretical observations translate to a reduced band gap for all the *para*-phenyl *meso*-substituted porphyrins.

The observed spectral changes as a function of *meso*-substitution are summarized by the following statements: The nitro and carboxy substitutions result in a reduction of the HOMO orbitals in comparison to the phenyl parent (TPP). The hydroxy substitution has minimal impact on the energy of the HOMO orbitals in comparison to the phenyl parent porphyrin. Regardless of the nature of the *para*-phenyl substituent, all substituted porphyrins exhibit lower energy LUMO and LUMO + 1 compared to TPP.

3.2. Transient absorption spectroscopy

Transient absorption spectroscopy for free-base substituted and unsubstituted porphyrins have been previously measured to analyze the ultrafast and long-lived nature of the photoinduced excited state.[29] To understand the influence porphyrin functionalization may have on the lifetime of these excited states, femtosecond transient absorption spectroscopy measurements were employed. Stabilization of the HOMO and/or LUMO through structural modifications, as suggested by TD-DFT calculations, can be supported through analysis of transient kinetics. According to previous reports, excitation of the Soret band for a free-base porphyrin leads to four decay processes on the femto and picosecond time scale as a result of sequential relaxation processes through the singlet and triplet states.[11,30] A diagram summarizing the aforementioned model is shown in Fig. 4. The first decay results from a quick depopulation of the singlet excited state of the Soret band (S2), (<50 fs), into a lower energy, singlet state Q_y, ($S_{1(Qy)}$) Subsequent relaxation to the singlet excited state of the Q_x band, ($S_{1(Qx)}$) also occurs rapidly (<100 fs) and therefore, is generally within the instrument response function (IRF) of many systems. It is suspected that within this established model, the shortest detectable component results from intramolecular vibrational energy redistribution (IVR) within the Q_x electronic band. The last kinetic time constant observable, considering the experimental delay line, corresponds to intersystem crossing (ISC) from the equilibrated $S_{1(Qx)}$- to the triplet (T_1) state; the lifetime of this relaxation is in the nanosecond time range.[11,30].

It should be noted that the dynamics of symmetrically substituted free-base porphyrins may be described using Soret, Q_x, and Q_y nomenclature when assigning the excited state due to the in-plane symmetry of the porphyrins within this study. For porphyrins of lower point group symmetry (i.e. asymmetrically substituted porphyrins), the transition dipole moment of the electronic

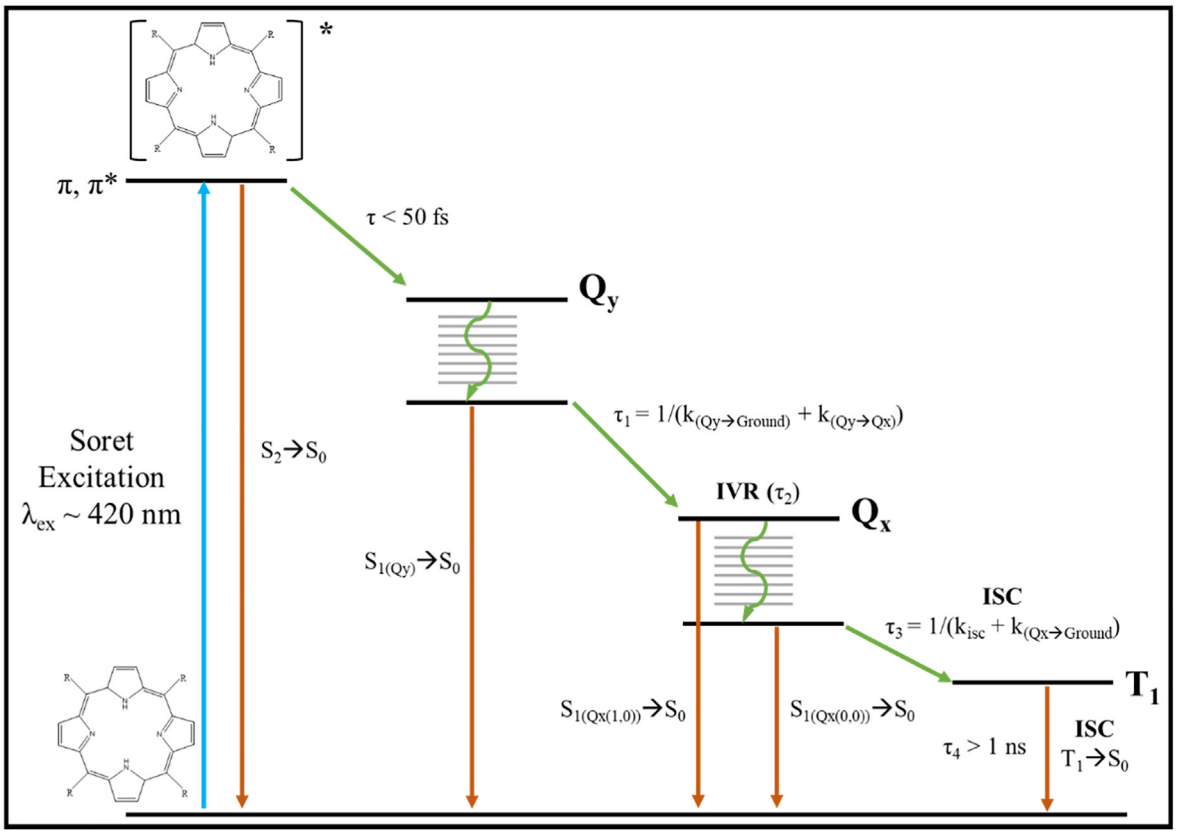

Fig. 4. Diagram of relaxation pathway of the excited state upon Soret band excitation of a free-base porphyrin based on experimental observations and literature sources [30].

transitions, described by the Gouterman four-orbital model,[28] no longer lie on the Cartesian axis of the porphyrin macrocycle. Therefore, the relaxed selection rules permit linear combinations of the one-electron excitations and mixing of the states. As a result of the ambiguity, the excited state should in those cases, be described by a designated and numbered singlet or triplet.[20].

This previous assessment of the excited state nature of free-base porphyrins paves the way for qualitative and quantitative analysis of the electronic impact of the porphyrin due to *meso*-substitution by directly monitoring the behavior of selected transient spectra and performing a global analysis.[30–31] Each of the free-base porphyrins were measured in THF upon Soret band excitation as a function of delay time between pump and probe up to 6 ns. Fig. 5 shows representative spectral slices for each system upon photoexcitation. The overall spectral shape is consistent with what has been previously reported for cyclic tetrapyrroles.[11,32] To aid in the assignment of the transient features, the time resolved spectrum (t = 1 ps) was overlaid with the steady-state absorption and emission spectra (Figure SI 11). This comparison clearly indicates that the minima observed in the transient absorption spectra for all porphyrins is directly in line with the steady-state absorption and fluorescence features of the Q-bands suggesting contribution of both ground state bleaching and stimulated emission. The main excited state absorption (ESA) band observed for the porphyrins has a maximum between 440 and 500 nm. In TPP and THPP, this transient appears to have the dominant feature with two peaks at around 470 nm and 490 nm.

The excited state photophysics of the selected free-base tetraphenyl porphyrins were analyzed using a global fitting analysis procedure using Surface Xplorer[9]. Fig. 6 shows the resulting global analysis and decay associated spectra (DAS) for all measured porphyrins to reveal the different contributing lifetimes to the overall spectrum; the extracted lifetimes are summarized in Table 2. In this analysis, the ultrafast relaxation, $S_2 \rightarrow S_1$, after initial Soret band excitation, was not able to be extracted given the IRF of 180 ps,[30] therefore the fitting model was reduced to a three component, unidirectional, parallel model described by two independent, competing processes: excited state decay and ground state recovery. The fit converged for all porphyrins with two significant components < 1 ps. However, for THPP, an appreciable short component (349 fs) was also extracted. This short lifetime is assumed to be the ultrafast relaxation from Q_y to Q_x, anoalogous to what has been reported for similar systems.[11] The subsequent resolvable process has been surmised in the literature to be solvent-induced IVR of the electron within the Q_x band.[30] According to our fitting model, this excited state relaxation occurs very quickly in TPP and THPP (7 ps and 10 ps, respectively), however, TCPP and TNPP reveal this lifetime to be fairly longer (27 ps and 14 ps, respectively). The following component of the excited state dynamics results from the overall singlet lifetime.[32] The extracted singlet lifetime for TPP was 12 ns, which is in line with previous reports.[33] Provided this model, the S_1 lifetime of the *meso*-substituted porphyrins with the carboxy or nitro groups was concluded to be 7 and 3 ns for TCPP and TNPP, respectively. THPP yielded a singlet lifetime of 7 ns; identical to that of TCPP. Analysis of the singlet lifetime requires consideration of two competing processes: ground state recovery ($S_1 \rightarrow S_0$) or intersystem crossing into the triplet state ($S_1 \rightarrow T$), as shown in Fig. 4. The results of the global analysis reveal that each of the porphyrins had a non-negligible contribution from the triplet state lifetime (τ = Inf) to the transient features. Therefore, the depopulation of the singlet state must be analyzed as a sum of these two different processes.

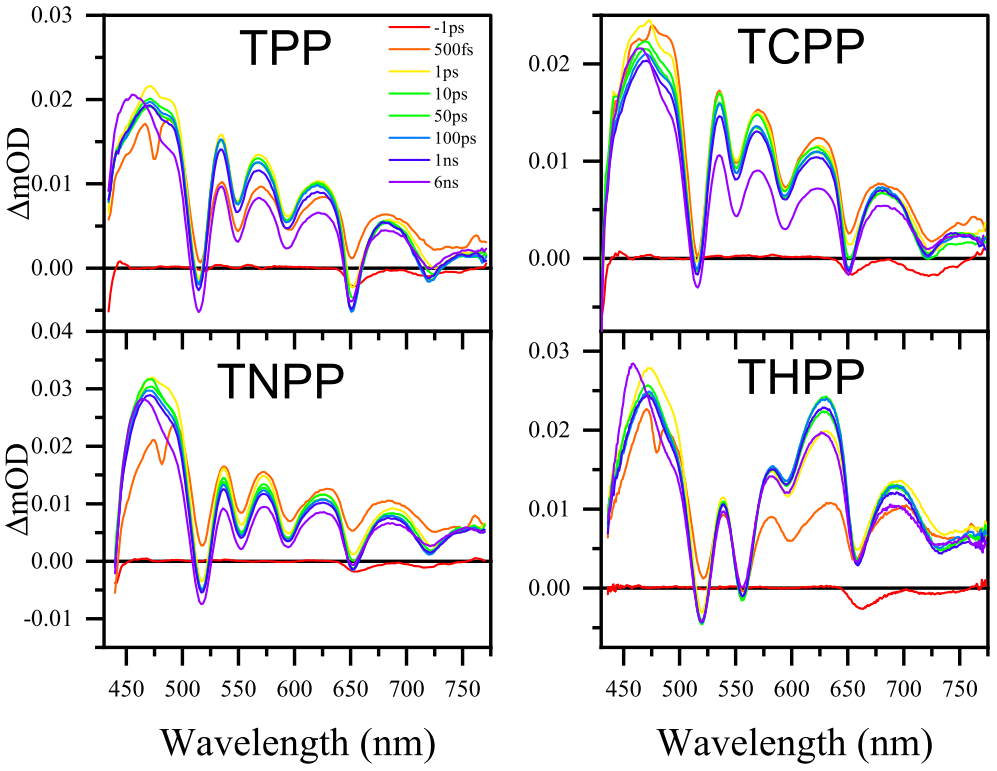

Fig. 5. Transient absorption spectroscopy spectra of TPP (A), TCPP (B), TNPP (C), and THPP (D) upon Soret band excitation.

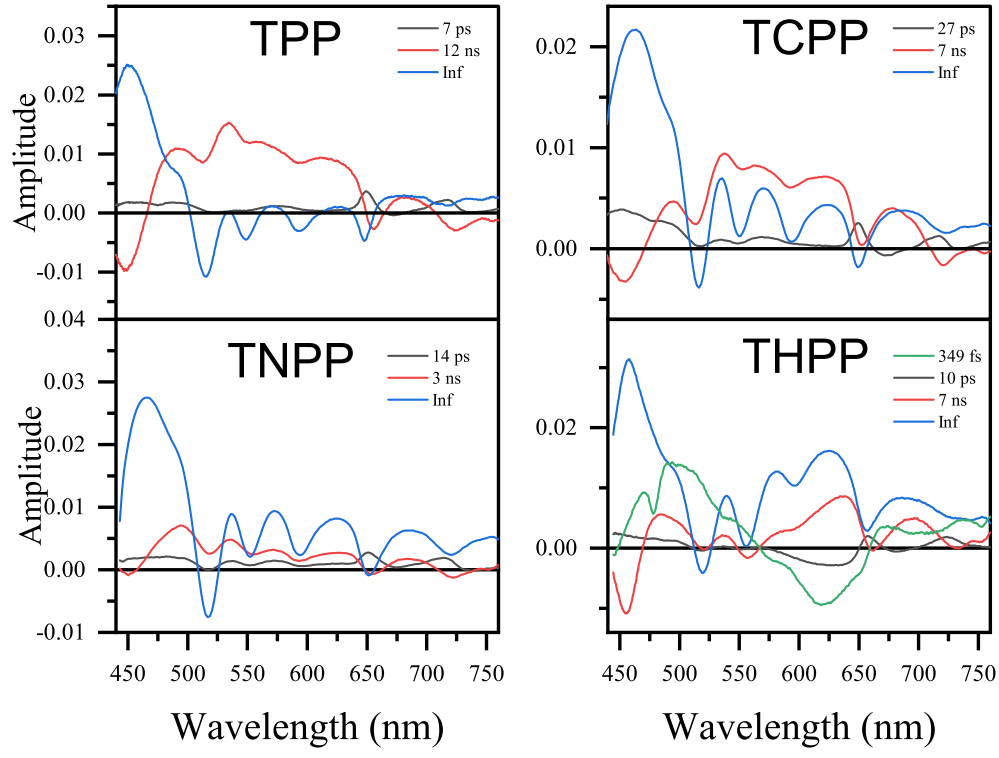

Fig. 6. Decay Associated Spectra (DAS) for Meso-substituted porphyrins.

Theoretical modeling, via TD-DFT calculations, aid in explaining how the various substituents alter the overall photophysics of the porphyrin. To understand the individual dynamics, the electronic spectrum was modeled using Gaussian 16,[10] implementing both singlet and triplet excitations using a previously reported computational prescription. The rate of intersystem crossing (k_{isc}) from the lowest singlet state to the triplet state was evaluated based on the energy gap law.[34] This law states that the rate of intersystem crossing is directly related to the relative energy difference between the two states involved in the transition, as well as the

Table 2
Extracted Lifetimes from Global Analysis.

Sample	IRF (ps)	τ_1 (ps)	τ_2 (ps)	τ_3 (ns)	τ_4
TPP	0.20	–	7 ± 3	12 ± 9	Inf
TCPP	0.20	–	27 ± 5	7 ± 4	Inf
TNPP	0.20	–	14 ± 3	3 ± 0.8	Inf
THPP	0.20	0.3 ± 0.1	10 ± 3	7 ± 5	Inf

magnitude of the spin–orbit coupling (SOC).[34–35] As shown in Table SI 2, the energies of the lowest lying singlet and triplet states were obtained through analysis of vertical excitation calculations performed on the selected porphyrins. The results indicate that TNPP has the smallest singlet/triplet energy gap of 0.71 eV. TCPP and THPP both were calculated to have ΔE = 0.73 eV followed by TPP with ΔE = 0.75 eV. This calculated trend corresponds inversely with the experimentally observed singlet lifetimes; TPP had the longest lifetime of 12 ns, followed by TCPP and THPP (7 ns), and then TNPP (3 ns). This observation supports the assumption that the photophysics of the singlet relaxation is partially a reflection of the orbital energy matching between the lowest singlet and triplet states, as described by the energy gap law. In summary, as the energy gap decreases, the rate of intersystem crossing increases yielding shorter singlet (S_1) lifetimes.

To comprehensively understand the differences in the singlet lifetime for the selected porphyrins, the contribution of the S_1 relaxation to the ground state must be considered. Previous studies indicates that excited state conformational changes promote $S_1 \rightarrow S_0$ relaxation and $S_1 \rightarrow T_1$ intersystem crossing, as observed in ruffled or saddled free-base porphyrins.[35] To reveal possible structural changes associated with photoexcitation, the Stokes shift in the steady-state absorption and emission spectra were evaluated. As shown in Table SI 3, the largest observed shift for the lowest energy transition, $Q_{x(0,0)}$, was observed in THPP (0.027 eV) whereas the other free-base porphyrins had relatively moderate shifts (0.010–0.016 eV). Additional evidence came from comparing the relative intensities and broadening of the fluorescence peaks. Similar to previous reports, the fluorescence features originating from the $Q_{x(0,0)}$ and $Q_{x(1,0)}$ transitions measured for THPP are noticeably broadened compared to the other porphyrins.[36] Furthermore, the relative intensity ratio of the two features deviates from that of the other porphyrins, in which the emission from the $Q_{x(0,0)}$ is drastically more intense than that from the $Q_{x(1,0)}$. The above observations suggest that the excited state may induce substantial structural changes in THPP which introduces enhanced Franck-Condon factors resulting in a reduced overlap of the ground and excited-state manifolds.[36] Large Stokes shifts between the steady-state electronic spectra and increased fluorescence quantum yield are experimental signatures of such excited state distortions.[36] These observations combined with the reduced triplet/singlet energy gap, can serve as a possible explanation for the observed photophysics of THPP that are distinct from those observed for the other porphyrins.

With the above conclusions in mind, the photophysics of Soret excitation for the selected free-base porphyrins can explained using a simple TD-DFT approach and aided with steady-state spectroscopy methods. The global analysis of the femtosecond transient absorption results reveals ultrafast processes with a long lived component (>1 ns) assigned to be the singlet (S_1) lifetime. The fitting model did account for an additional substantial component corresponding to the triplet lifetime ($\tau \sim$ infinite). The singlet kinetics as a function of substituent identity, can be understood by evaluating both the rate of intersystem crossing (k_{isc}) into the triplet state and the rate of ground state recovery.[37] The observed *para*-phenyl substituted porphyrins all yield shorter singlet lifetimes with respect to TPP. The reduction of the S_1 state lifetimes can explained using the energies of the singlet and triplet state calculated by TD-DFT. As defined by the energy gap law, the closer the orbital energy matching of the lowest singlet state and the triplet state, the faster ISC will occur. Given that the energy of the participating orbital in the $S_{1(Qx)} \rightarrow T_1$ transition is directly related to the substituent identity, the photophysics can be described as a function of the different phenyl groups. However, the excited state dynamics cannot be explained solely on the basis of inductive effect arguments. While the relative position of the LUMO and triplet states may be a product of stabilization due to the inductive effect, sterics play an important role in the different excited state dynamics. Experimental UV/Vis and fluorescence measurements allude to possible excited state structural distortions for THPP which may promote depopulation of the $S_{1(Qx)}$ state via ground state recovery ($S_{1(Qx)} \rightarrow S_0$). The lack of experimental evidence suggesting similar structural changes within TPP, TCPP, or TNPP suggest the decay pathway is primarily governed by the energy gap law.

3.3. Cyclic voltammetry and differential pulse voltammetry

The redox behavior of free-base porphyrins with various meso substituents has been studied via cyclic voltammetry.[5,38–39] These redox potentials were assigned to the one-electron addition or removal from the macrocycle of the porphyrin.[38] Provided this, the electrochemical properties of the substituted free-base porphyrins were investigated via cyclic voltammetry and differential pulse voltammetry to reveal changes in oxidation and reduction potentials as a function of the nature of the *meso*-substituent. The prepared porphyrin solutions were maintained air-free to prevent re-oxidation of the reduced species and prevent interference from ambient moisture. CV measurements were conducted using a glassy carbon working electrode, platinum wire counter electrode, and silver wire pseudo-reference electrode while a ferrocene/ferrocenium redox couple was used as an internal standard. DPVs were conducted in a similar fashion with the exception that the working electrode was a platinum button electrode. The resulting cyclic voltammograms and differential pulse voltammograms are shown in Figure SI 12 and Figure SI 13 and the extracted oxidation and reduction porphyrins, collected from both methods, are outlined in Table SI 4. The parent porphyrin, TPP, exhibits two, one electron redox couples with oxidation occuring at 1.33 V and 0.98 V followed by two clear reductions at −1.05 V and −1.42 V. The porphyrins bearing –COOH or $–NO_2$ the para position of the *meso*-substituted phenyl ring, TCPP and TNPP, both show two oxidations and two reductions. While the first oxidation potential for TCPP and TNPP are close in energy (0.77 V and 0.74), the second oxidation varies greatly, resulting in TNPP having a much larger ΔE_{ox} (0.50 V) than that of TCPP (0.18 V). The second reduction potential of both porphyrins is very similar, −1.39 V and −1.33 for TCPP and TNPP, respectively; however, the first reduction potentials are separated by 200 mV, with TCPP at −1.24 V and TNPP at −1.04 V. The hydroxyphenyl porphyrin, THPP, has two oxidations (0.93 V and 1.11 V) and two reduction potentials (-1.04 V and −1.28 V). CV measurements in the presence of ferrocene revealed an additional reaction around −0.5 V, in addition to the typical ferrocene and free-base porphyrin

oxidation and reduction peaks. (Figure SI 14) While elucidating the nature of this additional redox step is beyond the scope of this work, the electrochemical reaction between ferrocene and the free base porphyrin could be of future interest.

3.4. Spectroelectrochemical UV/Vis spectroscopy

Spectroelectrochemical UV/Vis studies were performed to observe the distinct spectral features associated with the charged version of the porphyrins in this study. As previously reported, electrochemical oxidation results in the formation of the π-dication of the porphyrin macrocycle.[38] To generate these species, the potential was held above the second oxidation maximum observed in the CV to ensure dication formation for each porphyrin (TPP: +1.3 V, THPP: +1.4 V, TCPP: +1.3 V, and TNPP: +1.5 V), as shown in Fig. 7. The parent TPP porphyrin reveals a red-shift in the Soret band from 418 nm for the neutral species, to 441 nm for the cationic porphyrin with an isosbestic point at approximately 428 nm. Additionally, this result is accompanied by a loss of both Q_y bands and a subtle increase in absorbance of both Q_x features. The *para*-substituted phenyl porphyrins, TCPP, TNPP, and THPP, all show similar behavior of the Soret band, in which the dicationic species is characterized by a shift to lower energy. In addition, both TNPP and TCPP lose all intensity of the Q_y bands. However, TNPP maintains two Q_x bands after oxidation, whereas TCPP only shows intensity in the $Q_{x(0,0)}$ band. The spectrum of the dicationic THPP exhibits only a $Q_{x(0,1)}$ and $Q_{x(0,0)}$ band in addition to the Soret band. In all oxidized porphyrins, the remaining Q-bands are also red-shifted with respect to the neutral species. Curiously, the spectra observed for all porphyrins are the same when holding the voltage at the first oxidation potential compared to when the voltage is held at the second oxidation potential (Figure SI 15). This observation suggests that dication formation may occur while holding the applied potential at the first observed oxidation in the CV, however, further study is needed to understand this observation.

The electrochemically generated anion and dianion species for each porphyrin exhibit similar spectral responses. To generate the anion and dianionic porphyrin, the potential was held above the first or second oxidation potential, respectively, to ensure formation of the species The formation of the mono-reduced porphyrin, depicted in Fig. 8, leads to the generation of a significantly red-shifted Soret band. THPP has the largest Soret band energy change (ΔE = 0.21 eV), followed by TNPP and TCPP (ΔE = 0.18 eV and ΔE = 0.17 eV, respectively). Similarly, the anionic TPP gives rise to a lower energy Soret band, but to a smaller extent (ΔE = 0.14 eV). Overall, generation of anionic porphyrin macrocycle results in a loss of both Q_y bands, independent of the *meso*-substituent. The Q_x bands shift and grow in intensity as the anion forms for all, except THPP, in which the $Q_{x(0,1)}$ band disappears.

Likewise, the spectral response of the formation of the dianion of each porphyrin was studied, as demonstrated in Fig. 9. As observed for the mono-anion, the substituted porphyrins exhibited a gradual loss of intensity of the Soret band and growth of a lower energy band. The trend in the red-shifting of the newly observed Soret band is: THPP > TNPP ~ TCPP > TPP. Additionally, electrochemical formation of the dianionic porphyrin results in similar Q-band behavior as observed for the anionic species. The spectroelectrochemical UV/Vis of the neutral, dicationic, and (di)anionic porphyrins are summarized in Table SI 5.

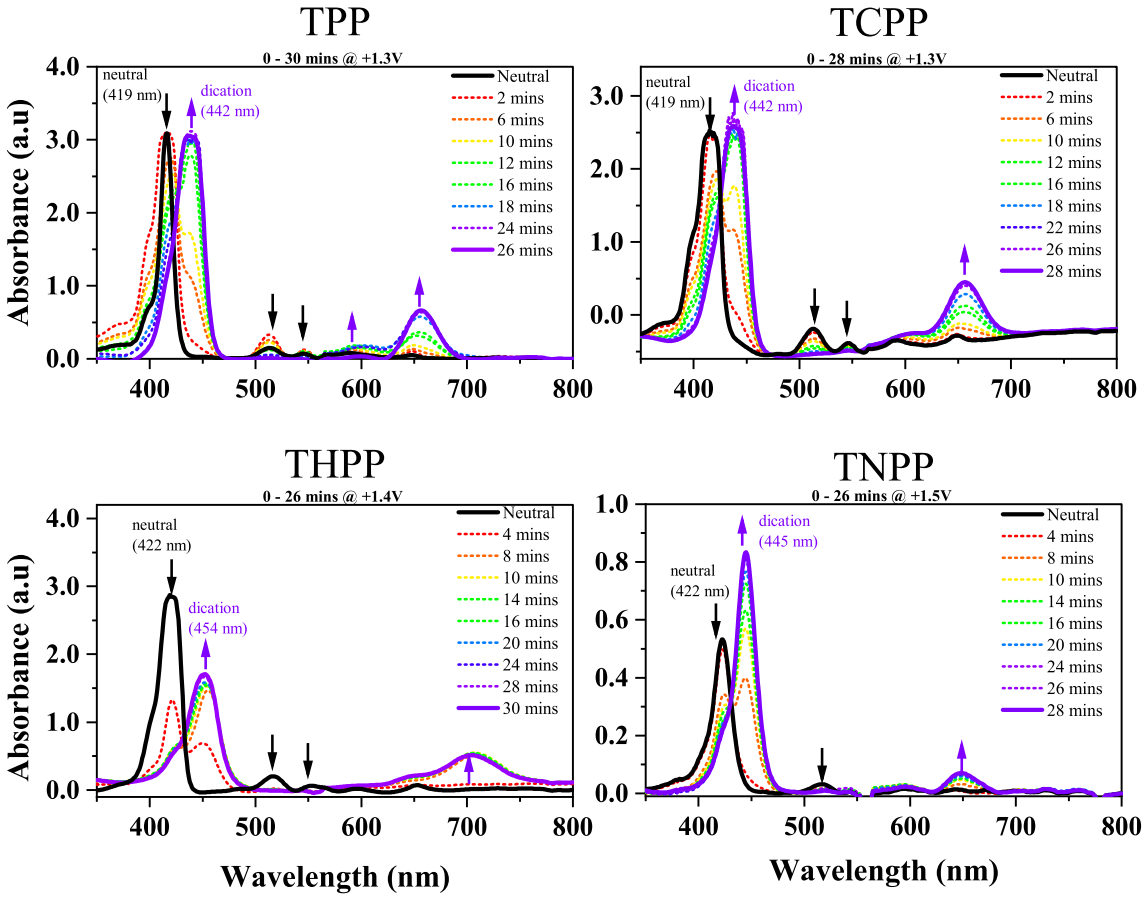

Fig. 7. Spectroelectrochemical UV/Vis spectra of TPP, TCPP, THPP, and TNPP and their dicationic species measured in THF.

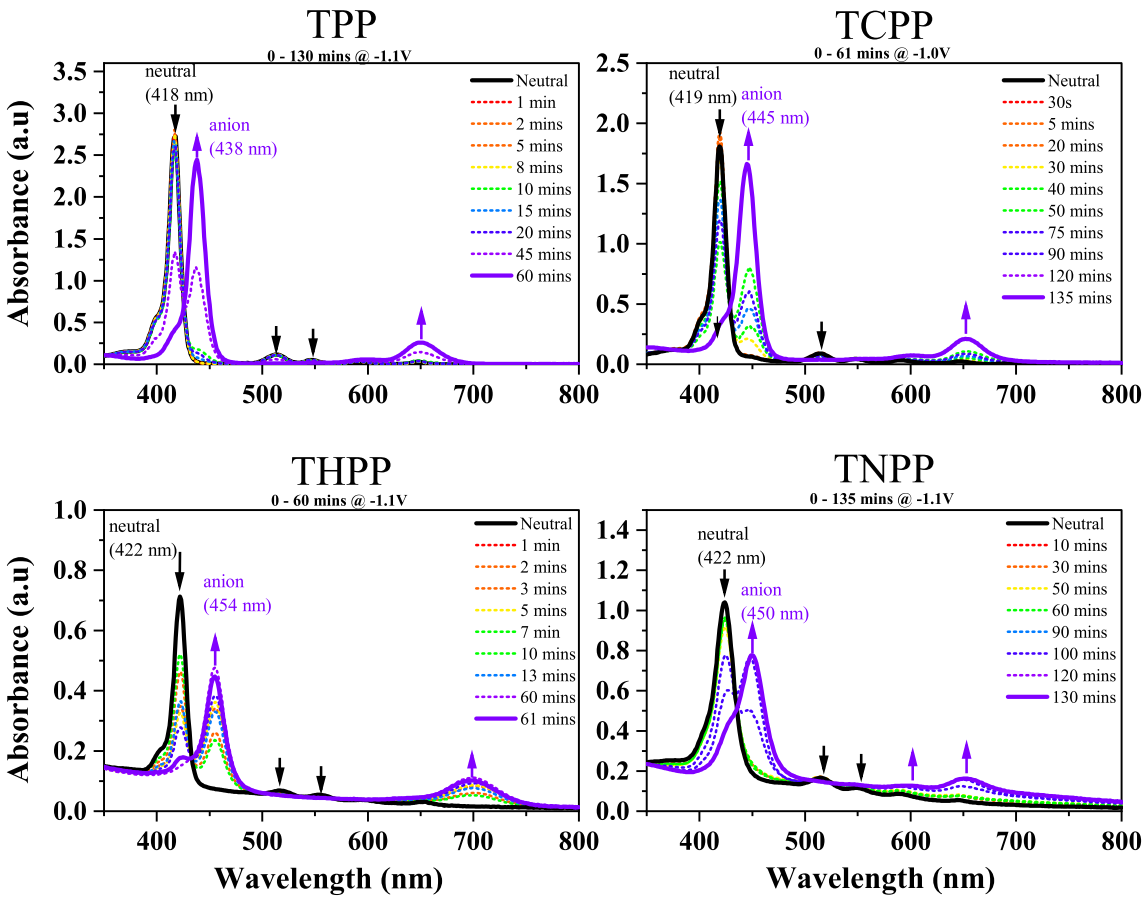

Fig. 8. Spectroelectrochemical UV/Vis spectra of TPP, TCPP,THPP,and TNPP and their monoanionic species measured in THF.

The spectral changes associated with the formation of the anionic and dicationic porphyrin species may derive from structural distortions resulting from the additional charge. As mentioned previously, the four Q-bands observed in free-base porphyrins pertain to vibronic transitions from the HOMO/HOMO-1 to the LUMO. [23] The intensity of these pseudo-dipole allowed transitions originate from the D2h symmetry of the planar, porphyrin macrocycle. Formation of the anionic, dianion, and dicationic species yields a red-shifted Soret band. Significant debate as to the origins red-shifts observed in various substituted neutral tetraaryl porphyrins has been discussed in previous work.[40] The origin of the observed red shifts in electronic spectra are believed to be from non-planar distortions of the macrocycle or relief of strain from in-plane nuclear reorganization (IPNR).[41–43] However, electronic effects such as increased conjugation of the *meso*-phenyl rings with the macrocycle as a result of the structural distortion, have been suggested.[44] DFT geometry optimizations performed in this work predict a substantial amount of saddling and distortion of the porphyrin core in the dicationic state. There are also substantial distortions in the porphyrin core predicted for TCPP, TNPP, and THPP dianions, but only minimal deviations from planarity for the monoanions and dianion of TPP. There are also corresponding bond length changes in all ionic porphyrin core bonds compared to the neutral species. It is likely that IPNR and porphyrin core distortions play a role in the observed red shift observed for the ionic species.

3.5. Electrochemical fluorescence spectroscopy

The fluorescence spectrum resulting from direct excitation of the Soret band in neutral, free base porphyrins results in two emission peaks corresponding to $Q_{x(0,0)}$ and $Q_{x(1,0)}$ radiative decays. [30,45–46] To elucidate how functionalization of the porphyrin influences the emission profiles of neutral and ionic species, fluoroesence spectra of the neutral, dication, anion, and dianion species were obtained. The results of these analyses are depicted in Fig. 10. The energies of the $Q_{x(0,0)}$ and $Q_{x(1,0)}$ bands are nearly identical for TPP, TCPP, and TNPP, but these features are red-shifted by about 10 nm for THPP. These observations are strikingly similar to the observed UV/Vis trends in which only THPP exhibited Q-bands that were substantially red-shifted, compared to the parent porphyrin, TPP.

In-situ electrochemical generation of the anionic and dicationic porphyrin reveals a notably different emission spectrum. The spectrum of all porphyrins, after applying the appropriate voltage, results in a new emission peak centered between the $Q_{x(0,0)}$ and $Q_{x(1,0)}$ bands with a smaller broad component at ~ 720 nm. Similar observations have been reported for the acid protonated dicationic free-base porphyrins in previous studies, however there remains ambiguity as to the origin of this emissive state.[46] The energy of the single observed emission peak for ionic TPP, THPP, TCPP, and TNPP species appears to be independent of whether an anionic or dicationic species is formed. Another notable observation is that the emission spectrum of the anionic and dicationic species for THPP are coincident in energy and significantly red-shifted compared to the neutral species. Interestingly, emission profiles consistent with the anionic species and neutral species are observed from neutral TCPP when excited in the range of 435–465 nm. (Figure SI 20) These observations are not surprising due to the weak acid nature of the carboxylic acid moieties and the equilibrium likely present between the protonated and deprotonated species of TCPP.

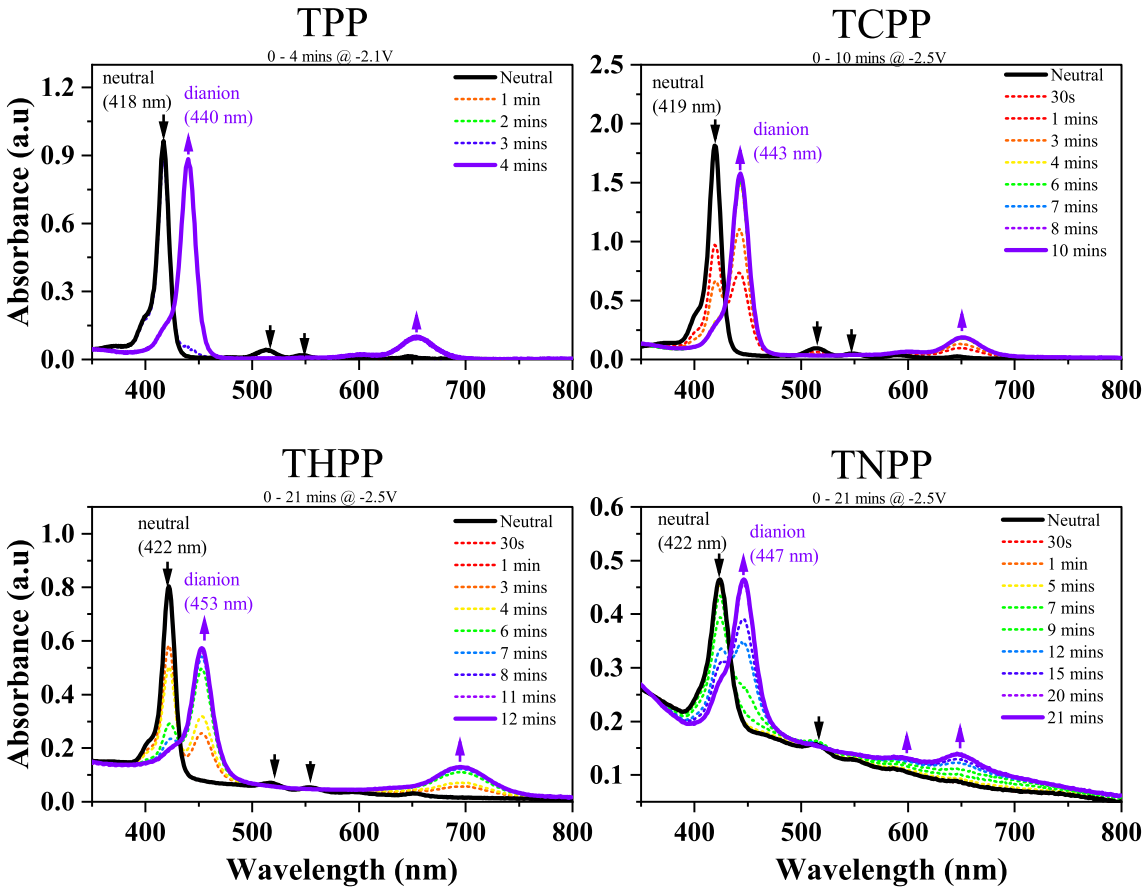

Fig. 9. Spectroelectrochemical UV/Vis of TPP, TCPP, THPP, and TNPP and their dianionic species measured in THF.

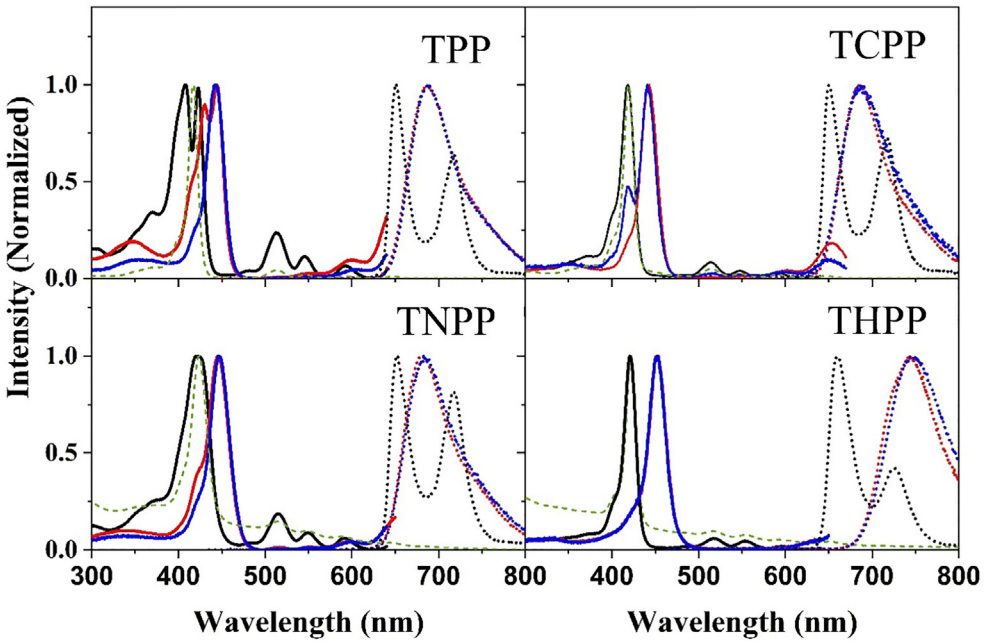

Fig. 10. Excitation (solid) and emission (dashed) spectrum of the different *meso*-substituted porphyrins for the neutral species (black), anion (red), and dication (blue). The neutral porphyrin UV/Vis spectrum is overlaid (green, dashed) for comparison.

The excitation profiles for the neutral porphyrins were collected by monitoring the dominate emission line in each porphyrin. For TPP, the transition pertaining to the Soret band, appears to be resolved into two different excitations, whereas TCPP, TNPP, and THPP only displayed one discernible transition. Aside from the Soret band, all porphyrins exhibited low intensity visible excita-

tions at similar energies to the Q-bands observed in the UV/Vis spectrum of the neutral porphyrin. Comparatively, the excitation spectrum was collected for the porphyrin dication and anion. The TPP anion has a split Soret band that is red-shifted compared to the neutral species. Generation of the dicationic TPP results in a merge of these features, resulting in a single Soret band. The observed Q-bands for ionic TPP solutions indicates the presence of only the Q_x bands, similar to the results of spectroelectrochemical UV/Vis measurements collected in Figs. 7-9. Likewise, the *para*-phenyl *meso*-substituted porphyrins all exhibited comparable excitation features to those revealed in the spectroelectrochemical UV/Vis studies.

4. Conclusions

A series of free base porphyrins served as models to evaluate the spectral and electrochemical changes observed upon incorporation of various functional groups to the para position of attached *meso*-substituted phenyl rings. Electronic structure changes observed through UV/Vis spectroscopy were interpreted through TD-DFT calculations and revealed that substitution on the *meso*-phenyl substituent with –COOH or $–NO_2$ groups (TCPP and TNPP) reduced the energy of both the HOMO-1 and HOMO, with respect to the parent TPP porphyrin. There was minimal effect on the energy of these frontier orbitals upon introduction of –OH (THPP) compared to TPP. The nearly degenerate LUMO and LUMO + 1 orbitals, regardless of the nature of the phenyl substituent, were lower in energy compared to TPP. These electronic effects were experimentally observed as moderate red shifts in the Q-bands for THPP, but very little change was observed in the carboxy or nitro group porphyrins. Further investigations using photoelectrochemical spectroscopy revealed spectral features associated with the formation of the anionic, dianionic, and dicationic species. Both anionic and cationic species displayed a red-shifted Soret band which was supported by TD-DFT calculations and believed to be related to both IPNR and porphyrin core distortions.

Analysis of the transient absorption spectroscopy measurements seem to correlate well with TD-DFT findings which lead to several conclusions on the photophysical nature of the *para*-substituted free-base meso tetraphenyl porphyrins. Excitation into the Soret band revealed a similar but complex excited state spectrum consisting of various overlapping excited state absorption, stimulated emission, and ground state bleaching bands. Global analysis indicated three different contributing lifetimes, the shortest being the ultrafast relaxation from Q_y to Q_x. Another fast component (10–22 ps) reflects the vibrational relaxation following the relaxation to $S_{1(Qx)}$. However, the longest component, corresponding to the lifetime of the singlet state ($S_{1(Qx)}$), revealed to be the largest deviation among the evaluated porphyrins. The decay of the singlet state is a sum of two competing processes but appears to be dominated by the rate of intersystem crossing into the triplet state. TCPP and THPP had identical singlet state decay lifetimes (7 ns), which is in sharp contrast to the extracted 3 ns singlet lifetime for TNPP. These lifetimes, revealed through global analysis, were all much shorter than the parent porphyrin, TPP (12 ns). Analysis of frontier molecular orbitals calculated using TD-DFT indicated a trend in the energy gap between the singlet and triplet states therefore, invocation of the energy gap law may provide a reasonable explanation for the drastic differences in the rate of ISC observed among these porphyrins. Additionally, analysis of the Stokes shift between the UV/Vis and fluorescence spectra suggests possible distortions of THPP in the excited state, which may promote a higher yield of ground state recovery though a $S_{1(Qx)} \rightarrow 0$ transition. Given these observations, it is clear that the photophysical dynamics of *meso*-substituted porphyrins are a function of many factors. However, the ultrafast dynamics indicate that small structural modifications, such as peripheral decoration of the macrocycle, can lead to drastically different relaxation dynamics.

Generation of the anionic, dianionic, and dicationic porphyrin species led to the generation of one primary fluorescence pathway from excitation into the Soret band in contrast to the two distinct emission pathways present for the neutral species. The emission was significantly red-shifted for the THPP porphyrin which correlates to the significantly red-shifted Q_x band in the electrochemical absorption spectra. The fluorescence emission observed for the TPP, TCPP, TNPP, and THPP anion and dication were strikingly similar in wavelength and peak profile. The detailed spectroscopic studies carried out in this work provides greater insight into the impacts of porphyrin functionalization on the spectroscopic signatures and electronic structure influences of free base porphyrins and their ions.

CRediT authorship contribution statement

Lauren Hanna: Writing – original draft, Investigation, Formal analysis, Visualization. **Edgar Movsesian:** Investigation. **Miguel Orozco:** Investigation. **Anthony R. Bernot Jr.:** Investigation. **Mona Asadinamin:** Investigation. **Learnmore Shenje:** Investigation. **Susanne Ullrich:** Supervision, Resources. **Yiping Zhao:** Supervision. **Nicholas Marshall:** Investigation, Resources, Formal analysis. **Jason A. Weeks:** Investigation, Formal analysis, Visualization. **Michael B. Thomas:** Investigation, Methodology. **Joseph A. Teprovich Jr.:** Investigation, Conceptualization, Methodology, Validation, Project administration, Formal analysis, Resources, Visualization, Supervision. **Patrick A. Ward:** Supervision, Conceptualization, Methodology, Investigation, Software, Funding acquisition, Project administration, Formal analysis, Resources, Visualization.

Declaration of Competing Interest

The authors declare that they have no known competing financial interests or personal relationships that could have appeared to influence the work reported in this paper.

Acknowledgements

This work was supported by the Laboratory Directed Research and Development (LDRD) program within the Savannah River National Laboratory (SRNL). This work was produced by Battelle Savannah River Alliance, LLC under Contract No. 89303321CEM000080 with the U.S. Department of Energy. Publisher acknowledges the U.S. Government license to provide public access under the DOE Public Access Plan (https://www.energy.gov/downloads/doe-public-access-plan). S.U. and L.S. acknowledge the National Science Foundation grant # CHE-1800050 for supporting instrumental capabilities utilized in this work.

Appendix A. Supplementary data

Supplementary data to this article can be found online at https://doi.org/10.1016/j.saa.2022.121300.

References

[1] J.L. McHale, Hierarchal Light-Harvesting Aggregates and Their Potential for Solar Energy Applications, J. Phys. Chem. Lett. 3 (2012) 587–597.
[2] Odobel, F. P., Y.; Warnan, J, Bio-Inspired Artificial Light-Harvesting Antennas for Enhancement of Solar Energy Capture in Dye-Sensitized Solar Cells. *Energy and Environmental Science* **2013,** *6*, 2041-2052.
[3] M. Chen, Chlorophyll Modifications and Their Spectral Extension in Oxygenic Photosynthesis, Annu. Rev. Biochem. 83 (2014) 317–340.

[4] R. Ma, P. Guo, H. Cui, X. Zhang, M.K. Nazeeruddin, M. Grätzel, Substituent Effect on the Meso-Substituted Porphyrins: Theoretical Screening of Sensitizer Candidates for Dye-Sensitized Solar Cells, J. Phys. Chemistry A 113 (37) (2009) 10119–10124.
[5] T.T.H. Tran, Y.-R. Chang, T.K.A. Hoang, M.-Y. Kuo, Y.O. Su, Electrochemical Behavior of meso-Substituted Porphyrins: The Role of Cation Radicals to the Half-Wave Oxidation Potential Splitting, J. Phys. Chem. C 120 (28) (2016) 5504–5511.
[6] A.D. Adler, F.R. Longo, J.D. Finarelli, J. Goldmacher, J. Assour, L. Korsakoff, A simplified synthesis for meso-tetraphenylporphine, J. Org. Chem. 32 (2) (1967) 476.
[7] Snellenburg, J. J.; Laptenok, S.; Seger, R.; Mullen, K. M.; van Stokkum, I. H. M., Glotaran: A Java-Based Graphical User Interface for the R Package TIMP. *2012* **2012,** *49* (3), 22.
[8] C. Slavov, H. Hartmann, J. Wachtveitl, Implementation and Evaluation of Data Analysis Strategies for Time-Resolved Optical Spectroscopy, Anal. Chem. 87 (4) (2015) 2328–2336.
[9] *Surface Xplorer*, 2019.
[10] Frisch, M. J.; Trucks, G. W.; Schlegel, H. B.; Scuseria, G. E.; Robb, M. A.; Cheeseman, J. R.; Scalmani, G.; Barone, V.; Petersson, G. A.; Nakatsuji, H.; Li, X.; Caricato, M.; Marenich, A. V.; Bloino, J.; Janesko, B. G.; Gomperts, R.; Mennucci, B.; Hratchian, H. P.; Ortiz, J. V.; Izmaylov, A. F.; Sonnenberg, J. L.; Williams; Ding, F.; Lipparini, F.; Egidi, F.; Goings, J.; Peng, B.; Petrone, A.; Henderson, T.; Ranasinghe, D.; Zakrzewski, V. G.; Gao, J.; Rega, N.; Zheng, G.; Liang, W.; Hada, M.; Ehara, M.; Toyota, K.; Fukuda, R.; Hasegawa, J.; Ishida, M.; Nakajima, T.; Honda, Y.; Kitao, O.; Nakai, H.; Vreven, T.; Throssell, K.; Montgomery Jr., J. A.; Peralta, J. E.; Ogliaro, F.; Bearpark, M. J.; Heyd, J. J.; Brothers, E. N.; Kudin, K. N.; Staroverov, V. N.; Keith, T. A.; Kobayashi, R.; Normand, J.; Raghavachari, K.; Rendell, A. P.; Burant, J. C.; Iyengar, S. S.; Tomasi, J.; Cossi, M.; Millam, J. M.; Klene, M.; Adamo, C.; Cammi, R.; Ochterski, J. W.; Martin, R. L.; Morokuma, K.; Farkas, O.; Foresman, J. B.; Fox, D. J. *Gaussian 16 Rev. C.01*, Wallingford, CT, 2016.
[11] M. Enescu, K. Steenkeste, F. Tfibel, M.-P. Fontaine-Aupart, Femtosecond relaxation processes from upper excited states of tetrakis(N-methyl-4-pyridyl)porphyrins studied by transient absorption spectroscopy, Phys. Chem. Chem. Phys. 4 (24) (2002) 6092–6099.
[12] M.D. Hanwell, D.E. Curtis, D.C. Lonie, T. Vandermeersch, E. Zurek, G.R. Hutchison, Avogadro: An advanced semantic chemical editor, visualization, and analysis platform, J. Cheminformatics 4 (1) (2012).
[13] A.D. Becke, J. Chem. Phys. 98 (1993) 5648–5652.
[14] C. Lee, W. Y., R.G. Parr, *Phys. Rev. B* **1988,** *37*, 785-789.
[15] P.J. Stephens, F. J. D., C.F. Chabalowski, M.J. Frisch, **1994,** *98*, 11623-11627.
[16] S.H. Vosko, L. W., M. Nusair, *Can. J Phys.* **1980,** *58*, 1200-1211.
[17] R. Krishnan, J.S. Binkley, R. Seeger, J.A. Pople, Self-consistent molecular orbital methods. XX. A basis set for correlated wave functions, J. Chem. Phys. 72 (1) (1980) 650–654.
[18] K.V. Shrestha, A. Kyle, Jakubikova, Elena, Electronic Absorption Spectra o Tetrapyrrole-Based Pigments via TD-DFT: A reduced Orbital Space Study, J. Phys. Chem. A 120 (2016) 5816–5825.
[19] Roy D. Dennington II, T. A. K. a. J. M. M. *GaussView*, 6.1.1; Semichem, Inc. : 2000-2019.
[20] A.K. Mandal, M. Taniguchi, J.R. Diers, D.M. Niedzwiedzki, C. Kirmaier, J.S. Lindsey, D.F. Bocian, D. Holten, Photophysical Properties and Electronic Structure of Porphyrins Bearing Zero to Four meso-Phenyl Substituents: New Insights into Seemingly Well Understood Tetrapyrroles, J. Phys. Chem. A 120 (49) (2016) 9719–9731.
[21] A.H. Corwin, A.B. Chivvis, R.W. Poor, D.G. Whitten, E.W. Baker, Porphyrin studies. XXXVII. The interpretation of porphyrin and metalloporphyrin spectra, J. Am. Chem. Soc. 90 (24) (1968) 6577–6583.
[22] M. Gouterman, Spectra of porphyrins, J. Molecular Spectroscopy 6 (1961) 138–163.
[23] Spellane, P. J.; Gouterman, M.; Antipas, A.; Kim, S.; Liu, Y. C., Porphyrins. 40. Electronic spectra and four-orbital energies of free-base, zinc, copper, and palladium tetrakis(perfluorophenyl)porphyrins. *Inorg. Chem.* **1980,** *19* (2), 386-391.
[24] J.R. Weinkauf, S.W. Cooper, A. Schweiger, C.C. Wamser, Substituent and Solvent Effects on the Hyperporphyrin Spectra of Diprotonated Tetraphenylporphyrins, J. Phys. Chem. A 107 (18) (2003) 3486–3496.
[25] Y. Cui, L. Zeng, Y. Fang, J. Zhu, H.-J. Xu, N. Desbois, C.P. Gros, K.M. Kadish, Electrochemical and Spectroelectrochemical Properties of Free-Base Pyridyl- and N-Alkyl-4-Pyridylporphyrins in Nonaqueous Media, ChemElectroChem 3 (1) (2016) 110–121.
[26] J.M.S. Lopes, J.R.T. Reis, A.E.H. Machado, T.H.O. Leite, A.A. Batista, T.V. Acunha, B.A. Iglesias, P.T. Araujo, N.M. Barbosa Neto, Influence of the meso-substituents on the spectral features of free-base porphyrin, Spectrochim. Acta, Part A 238 (2020) 118389.
[27] J. Šeda, J.V. Burda, J. Leszczynski, Study of electronic spectra of free-base porphin and Mg-porphin: Comprehensive comparison of variety of ab initio, DFT, and semiempirical methods, J. Comput. Chem. 26 (3) (2005) 294–303.
[28] M. Gouterman, Study of the Effects of Substitution on the Absorption Spectra of Porphin, J. Chem. Phys. 30 (5) (1959) 1139–1161.
[29] R.F. Khairutdinov, N. Serpone, Photoluminescence and Transient Spectroscopy of Free Base Porphyrin Aggregates, J. Phys. Chem. B 103 (5) (1999) 761–769.
[30] J.S. Baskin, H.-Z. Yu, A.H. Zewail, Ultrafast Dynamics of Porphyrins in the Condensed Phase: I. Free Base Tetraphenylporphyrin, J. Phys. Chem. A 106 (42) (2002) 9837–9844.
[31] A. Marcelli, P. Foggi, L. Moroni, C. Gellini, P.R. Salvi, Excited-State Absorption and Ultrafast Relaxation Dynamics of Porphyrin, Diprotonated Porphyrin, and Tetraoxaporphyrin Dication, J. Am. Chem. Soc. 112 (9) (2008) 1864–1872.
[32] P.H. Kumar, Y. Venkatesh, D. Siva, B. Ramakrishna, P.R. Bangal, Ultrafast Relaxation Dynamics of 5,10,15,20-meso-Tetrakis Pentafluorophenyl Porphyrin Studied by Fluorescence Up-Conversion and Transient Absorption Spectroscopy, J. Phys. Chem. A 119 (8) (2015) 1267–1278.
[33] M. Taniguchi, J.S. Lindsey, D.F. Bocian, D. Holten, Comprehensive review of photophysical parameters (ε, Φf, τs) of tetraphenylporphyrin (H2TPP) and zinc tetraphenylporphyrin (ZnTPP) – Critical benchmark molecules in photochemistry and photosynthesis, J. Photochem. Photobiol., C 46 (2021) 100401.
[34] S. Perun, J. Tatchen, C.M. Marian, Singlet and Triplet Excited States and Intersystem Crossing in Free-Base Porphyrin: TDDFT and DFT/MRCI Study, ChemPhysChem 9 (2) (2008) 282–292.
[35] S. Gentemann, C.J. Medforth, T. Ema, N.Y. Nelson, K.M. Smith, J. Fajer, D. Holten, Unusual picosecond 1(π, π*) deactivation of ruffled nonplanar porphyrins, Chemical Physics Letters 245 (4) (1995) 441–447.
[36] J.-H. Ha, S.I. Yoo, G.Y. Jung, I.R. Paeng, Y.-R. Kim, Substitution effect of hydroxyl group on photophysical properties of tetraphenylporphyrin (H2TPP) and germanium(IV) tetraphenylporphyrin dichloride (Ge(IV)TPPCl2), J. Mol. Struct. 606 (1) (2002) 189–195.
[37] Y. Venkatesh, M. Venkatesan, B. Ramakrishna, P.R. Bangal, Ultrafast Time-Resolved Emission and Absorption Spectra of meso-Pyridyl Porphyrins upon Soret Band Excitation Studied by Fluorescence Up-Conversion and Transient Absorption Spectroscopy, J. Phys. Chem. B 120 (35) (2016) 9410–9421.
[38] C. Inisan, J.-Y. Saillard, R. Guilard, A. Tabard, Y. Le Mest, Electrooxidation of porphyrin free bases: fate of the π-cation radical, J. Chemistry 22 (8) (1998) 823–830.
[39] K.M. Kadish, M.M. Morrison, Solvent and substituent effects on the redox reactions of para-substituted tetraphenylporphyrin, J. Am. Chem. Soc. 98 (11) (1976) 3326–3328.
[40] H. Ryeng, A. Ghosh, Do Nonplanar Distortions of Porphyrins Bring about Strongly Red-Shifted Electronic Spectra? Controversy, Consensus, New Developments, and Relevance to Chelatases, J. Am. Chem. Society 124 (27) (2002) 8099–8103.
[41] A.K. Wertsching, A.S. Koch, S.G. DiMagno, On the Negligible Impact of Ruffling on the Electronic Spectra of Porphine, Tetramethylporphyrin, and Perfluoroalkylporphyrins, J. Am. Chem. Soc. 123 (17) (2001) 3932–3939.
[42] S. Zakavi, R. Omidyan, S. Talebzadeh, Porphine core saddling: Effects on the HOMO/LUMO gap and the macrocycle bond lengths and bond angles, Polyhedron 49 (1) (2013) 36–40.
[43] R.E. Haddad, S. Gazeau, J. Pécaut, J.-C. Marchon, C.J. Medforth, J.A. Shelnutt, Origin of the Red Shifts in the Optical Absorption Bands of Nonplanar Tetraalkylporphyrins, J. Am. Chem. Soc. 125 (5) (2003) 1253–1268.
[44] A. Rosa, G. Ricciardi, E.J. Baerends, A. Romeo, L. Monsù Scolaro, Effects of Porphyrin Core Saddling, meso-Phenyl Twisting, and Counterions on the Optical Properties of meso-Tetraphenylporphyrin Diacids: The [H4TPP](X)2 (X = F, Cl, Br, I) Series as a Case Study, J. Physical Chem. A 107 (51) (2003) 11468–11482.
[45] J.R.C. Weinkauf, W. Sharon, A. Schweiger, C.C. Wamser, Substituent and Solvent Effects on the Hyperporphyrin Spectra of Diprotonated Tetraphenylporphyrins, J. Phys. Chem. A 107 (2003) 3486–3496.
[46] S. Zakavi, S. Hoseini, The absorption and fluorescence emission spectra of meso-tetra(aryl)porphyrin dications with weak and strong carboxylic acids: a comparative study, RSC Adv 5 (129) (2015) 106774–106786.